Indian Journal of Chemical Technology
Vol. 32, March 2025, pp. 230-240
DOI: 10.56042/ijct.v32i2.11071

Adsorptive removal of malachite green using fox nutshell activated carbon: Adsorption isotherms and kinetic study

Abhishek Srivastava[1], Ruchi Singh[2] & Neetu Srivastava[3]*

[1]Department of Chemistry, GLA University, Mathura-281006, U.P., India

[2]Department of Chemistry, B. N College of Engineering & Technology, Lucknow, U.P., India

[3]Department of Chemistry, Deen Dayal Upadhyay Gorakhpur University, Gorakhpur-273009, U.P., India

*E-mail: neetusrivastav25@gmail.com

Received 11 May 2024; accepted 13 January 2025

Over the past few years, environmental concerns regarding dye contamination have grown. Removing dye from wastewater from industry is crucial for environmental sustainability. Fox nutshell, an agricultural byproduct, is widely available in India. Its fibrous texture and high cellulose, hemicellulose, and lignin content make it ideal for dye adsorption. By zinc chloride activation followed by carbonization at 600 ℃, fox nutshell has been converted into low-cost fox nutshell activated carbon (FNAC). Its ability to adsorb malachite green (MG) from aquatic solutions is investigated. A porous framework with 2408.9 m^2/g surface area and 2.51 nm average pore diameter is discovered in the FNAC using SEM, and BET investigations. FTIR analysis shows the presence of the –COOH, C=C, C=O, and –OH, functional groups on the surface of FNAC. The adsorption system adhered to a pseudo-second-order kinetic model, with the equilibrium time being determined at 90 min. The Langmuir model accurately simulated the adsorption isotherms. The optimum pH for MG (500 mg/L) adsorption onto FNAC (0.08 gm/100 mL) was 6.5, with an adsorption capacity of 523.3 mg/g at 298 K. Negative ΔG° and ΔH° indicate spontaneous MG adsorption onto FNAC, decreasing with temperature. π–π interactions, electrostatic attractions, and hydrogen bonding amongst the FNAC functional groups and the MG lead to the potential adsorption of MG.

Keywords: Activated carbon, Fox nutshell, Kinetic modeling, Langmuir adsorption isotherm, Malachite green

Introduction

Water pollution is a significant and enduring challenge that has plagued human society across the ages. Its detrimental impact on the health and well-being of billions of individuals globally is undeniable, leading to the emergence of many diseases including cholera, diarrhea, and cancer[1, 2]. Moreover, water pollution has been linked to adverse effects on vital organs such as the skin, lungs, brain, kidneys, and liver[1, 2]. A plethora of infectious and harmful contaminants, such as radioactive elements, heavy metal ions, dyes, and pesticides, can be found in copious quantities of wastewater[3,4]. The primary contributors to wastewater contamination are organic dyes derived from paper, pulp, leather, food, pharmaceuticals, textiles, paints, and coating industries[5,6]. Cost-effective and efficient procedures and techniques are crucial for the removal of hazardous dyes from wastewater due to their significant implications for public health and the preservation of aquatic ecosystems[7]. In order to effectively eliminate dyes from aqueous solutions and wastewater, numerous methodologies have been commonly utilized, encompassing adsorption, coagulation, microfiltration, nano-filtration, photo-catalysis, ozonation, electro-chemistry, aerobic and anaerobic microbial degradation, membrane separation, oxidative degradation, and chemical oxidation[8-13].

The World Health Organization (WHO) has reported that 17-20% of the pollution of industrial water is caused by textile dyeing processes. The textile dyeing industry uses about 80% of azo dyes, and 10-15% are lost through wastewater without binding to fiber[14,15]. The ineffective degradation performance of cationic dyes by conventional biochemical treatments can be attributed to the presence of aromatic rings within their structure[16]. Malachite green is a solid, crystalline, cationic dye[17,18]. The growing demand for malachite green in multiple industries is due to its higher stability, synthetic nature, high water solubility, and affordability[19]. It is extensively used in manufacturing sectors such as silk, wool, paint, pulp and paper, food, leather, and textile dying[20]. Malachite green is also employed as a fungicide, parasiticide, and antiseptic[21]. Nevertheless, malachite green dye is linked to both environmental and human health concerns. This

compound has long-lasting effects, builds up in living organisms, causes genetic mutations, is linked to cancer, and can cause birth defects[22,23]. Ingesting malachite green through water can have serious health effects on vital organs such as the kidneys, heart, and breasts[23]. Therefore, humanity as a whole has made the removal of persistent dyes like malachite green a top priority in order to preserve the environment and protect human health.

Activated carbon finds widespread use as an adsorbent in several applications related to wastewater treatment. The material exhibits a significantly enhanced level of porosity, showcasing a substantial internal surface area, and demonstrating commendable mechanical strength[24-26]. Even though it's extensive utilization across various industries, activated carbon continues to be a material of considerable cost. Hence, it becomes imperative to conduct an in-depth exploration and advancement of cost-efficient carbon materials that can be effectively utilized for the purpose of mitigating water pollution. A diverse range of cost-effective materials has been employed for the purpose of extracting malachite green from aquatic solutions. These materials encompass lantana camara L. stem, nutraceutical industrial fenugreek seed, okra stalks waste, stipatenacissima L. leaf powder, cocosnucifera shells, walnut shells, *heveabrasiliensis* root, cathaedulis stem, almond shell, jackfruit peel salaccazalacca, and rumex abyssinicus[27-36]. Many researchers are interested in this low-cost adsorption approach because it doesn't require a sophisticated regeneration methodology. Euryale ferox is a plant that thrives in tropical and subtropical climates. It is a well-known agricultural by-product, commonly referred to as Makhana. This aquatic herb belongs to the water lily family (Nymphaeaceae). Although E. ferox originated in the East Indies, it has been widely cultivated for a long time all over the world. E. ferox has been frequently utilized in traditional medicine to treat a range of ailments, such as excessive leucorrhoea, chronic diarrhea, and kidney problems[37]. Despite the abundance of E. ferox, their shells have historically been utilized as fuel. A recent study has discovered a new use for E. ferox shells in the production of activated carbon. This involves utilizing $ZnCl_2$, KOH, and H_3PO_4 as chemical activation agents[38-41].

Our research aims to evaluate the effectiveness of using fox nutshell activated carbon (FNAC) in removing MG dye from wastewater. The investigation of FNAC properties involves the utilization of numerous analytical techniques, including FTIR, BET, and SEM. The investigation encompassed an examination of the impact of different operating parameters, including contact time, adsorbent dose, initial MG concentration, temperature, and pH of the solution. The investigation focused on studying adsorption isotherms, employing various adsorption models such as the Langmuir, and Freundlich. Additionally, kinetic models (pseudo-second-order, Intra-particle diffusion, and pseudo-first-order) were employed to assess the experimental data and gain insights into the adsorption behavior of MG onto FNAC. Thermodynamic investigations were also conducted to assess the enthalpy change (ΔH^o), standard free energy (ΔG^o), and entropy change (ΔS^o) in order to ascertain the nature of the adsorption phenomenon (endothermic or exothermic).

Experimental Section

Materials and Method

All experiment was conducted using double-deionized water (DDW) and analytical-grade reagents over the entire study. Zinc chloride (AR, Fisher Scientific, India), and malachite green oxalate salt (AR, Merck, India) utilized were of utmost purity. The stock solution of 1000 mg/L of MG was prepared in double distilled water (DDW). NaOH (Fisher Scientific, India), and HCl (Merck, India) solutions were employed to modulate the pHemployinga Systronics 361 pH meter. FT-IR spectrophotometer (IR Affinity, Shimadzu) was utilized to examine the functional groups in FNAC. Utilizing a scanning electron microscope (S4800, Hitachi, Japan), FNAC's surface morphology was observed, while BET was used to determine the surface area of the prepared FNAC.

Preparation of FNAC

The fox nutshell (FNS) was collected from the Hardoi district of Uttar Pradesh (India). After washing thoroughly with DDW, FNS was soaked in 0.4 M NaOH solution and left overnight to eliminate impurities. Thereafter it was thoroughly rinsed with distilled water until the pH of the rinsed solution reached approximately 7. After drying at 110°C for 20 h, the residue was ground and sieved to obtain the fox nut shell powder (FNSP) of the desired particle size (100 μm). Approximately 50 g of $ZnCl_2$ were dispersed in 150 mL of distilled water, followed by the addition of 20 g of FNSP at a temperature of 80°C. The mixture was stirred once every six hours during the course of the mixture's 24 h sitting at room temperature.

Following that, the soaked sample was dried at 110°C for 24 h in a hot oven. Carbonization of the obtained dried material was performed at 600°C for 60 min in an electric tubular furnace tube in an N_2 environment. Once the procedure is finished, the resulting combustion material is immersed in 0.4 N HCl for a duration of 24 h. The carbonized material has been thoroughly rinsed multiple times using hot DDW and then cold DDW till the water pH utilized for washing has become neutral. The moist substance has been dehydrated in an oven for 24 h at 110°C and placed in sealed plastic bags for storage.

Malachite Green Adsorption Experiments

The optimal parameters for MG adsorption on FNAC were found by conducting adsorption investigations using FNAC. For that, the calculated amount of FNAC (0.08 g to 0.8 g) and 100 mL MG solution (100 to 500 mg/L) were carefully introduced into a 250 mL round bottom flask. HCl or NaOH solution was utilized to maintain the pH of the reacting mixture prior to the addition of the adsorbent. The test solutions were then shaken for 140 min at 150 rpm in a thermostat rotator while maintaining a consistent temperature of 298 K. Subsequently, the supernatant solutions obtained via centrifugation underwent filtration, and the quantification of MG content in each flask was accomplished utilizing a Spectronic 20D (Milton Roy Co.) visible spectrophotometer at a wavelength of 617 nm, which corresponds to the maximum absorbance (λ_{max}) for MG. The uptake of MG at equilibrium, q_e (mg/g), and the % removal of MG were determined using Eqs 1 and 2.

$$q_e = \frac{(C_o - C_e) \times V}{m} \quad ...(1)$$

$$\text{Percentage Removal} = \frac{(C_o - C_e) \times 100}{C_o} \quad ...(2)$$

Where, the variables are the initial concentration of MG (C_o), the equilibrium concentration of MG (C_e), the mass of the adsorbent (m), and the volume of the solution (V).

Results and Discussion

Characterization of FNAC

Fig. 1a shows the SEM image of FNAC powder prior to adsorption. The image exhibits an asymmetric, rough, and porous structure. In addition, it has micro-sized active sites or cavities, indicating that FNAC powder shows great potential as an adsorbent for effectively capturing MG. One of the most significant characteristics of adsorbents is their surface area. Fig. 1b represents the nitrogen adsorption-desorption isotherms for prepared FNAC. It was discovered that FNAC had a surface area of 2408.9 m^2/g, which was comparatively large for the effective adsorption of dyes. The average pore diameter of 2.51 nm suggests the mesoporous structure of FNAC[39, 42]. Using the KBr pellet method, the FT-IR spectra of FNAC have been scanned in the 4000-700 cm^{-1} wavenumber region. The FT-IR spectra of FNACis shown in Fig. 2. The FTIR spectra of FNAC revealed that the absorbance bands had peaks at 3372, 2938, 1728, 1635, 1448, 1371, 1241, 1160, and 1041 cm^{-1}. Other researchers have documented the majority of these bands for various carbon compounds. A band between 3500-3300 cm^{-1}

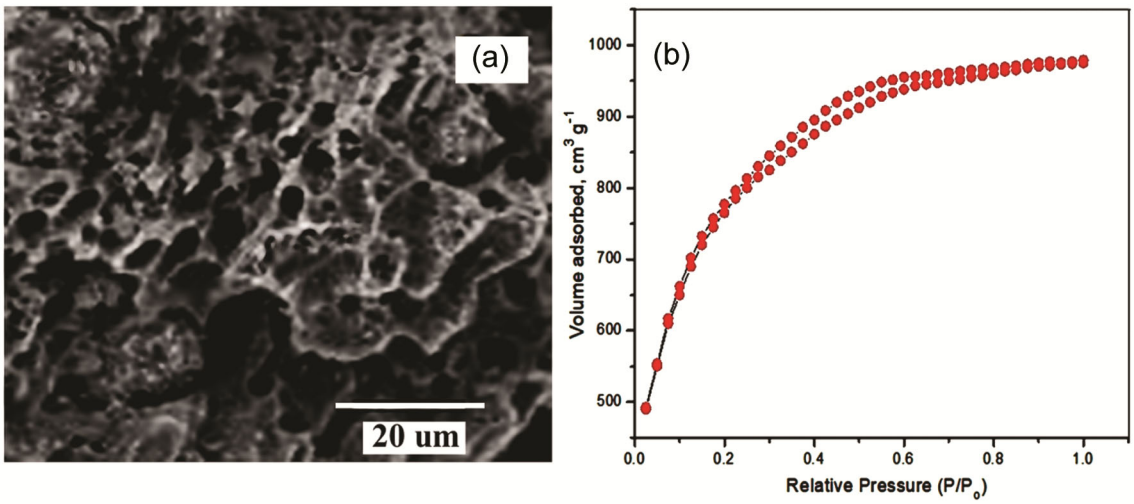

Fig. 1 — (a) SEM image and (b) Nitrogen adsorption-desorption isotherms for prepared FNAC

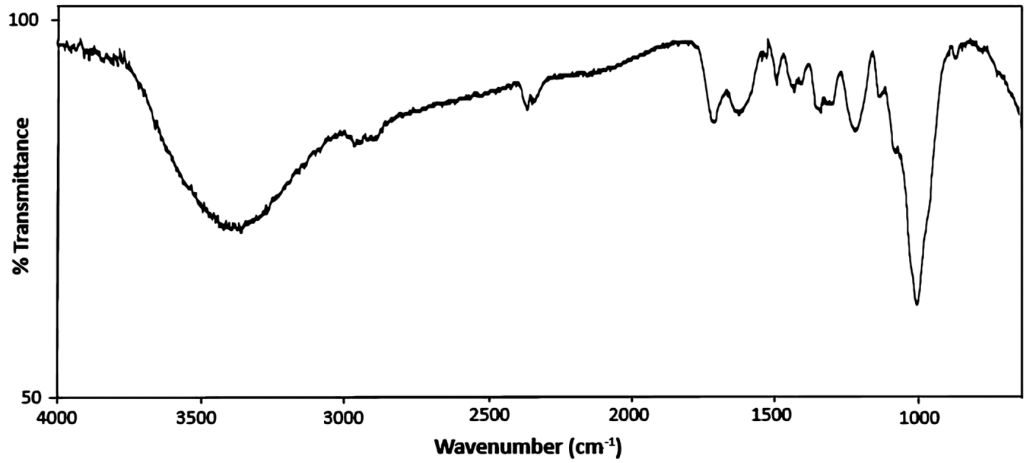

Fig. 2 — FT-IR spectra of FNAC

can be ascribed to -OH stretching[39,40]. A peak between 3000-2875 cm^{-1} corresponds to alkane C-H stretching. At 1728 cm^{-1}, we observe the distinctive C=O stretching of the carboxylic acid group[41]. Peaks at 1635 and 1448 cm^{-1} are indicative of sp^2-hybrid carbon-carbon (C=C, stretching) and O-H bending, respectively[40]. A peak at 1240, 1160, and 1030 cm^{-1} indicates C-O stretching and O-H bending vibrations of distinct functional groups (ethers, esters, and alcohols)[40]. The presence of the –COOH, C=C, C=O, and –OH groups indicates that there has been a significant amount of interaction between the adsorbate and the adsorbent, which could help MG adsorb onto the FNAC's active sites.

Influence of pH on MG Removal

The primary variable influencing adsorption efficacy is pH because it influences the interface properties of the adsorbate and adsorbent by altering the surface charge, the behaviour of the adsorbate in the reaction mixture, and deprotonation/protonation of the distinct functional groups on the adsorbent surface[40]. The adsorption investigation was performed in the pH ranging from 2.0 to 9.0, as illustrated in Fig. 3. MG adsorption by FNAC was extremely pH sensitive; when the pH level rose from 2.0 to 6.5, the removal efficacy increased rapidly from 45.3% to 98.8%, with further change in pH values from 6.5 to 9.0, the percentage removal of MG has been decreased down to 61.2%. Therefore, the subsequent experiments have been performed at pH 6.5. There are multiple factors contributing to the outcome of the solution's pH on the MG adsorption on FNAC. Controlling electrostatic interactions between the adsorbent and adsorbate is a crucial factor to consider.

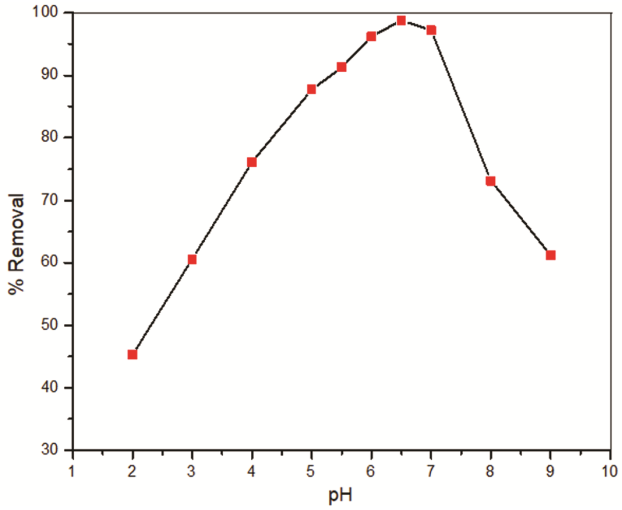

Fig. 3 — Influence of pH on % removal of MG at [MG] = 100 mg/L, FNAC dose = 0.08 g/100 ml, Temperature = 298 K, and Contact time = 140 min

The reduced removal percentage at lower pH reflects the protonation of MG in acidic conditions. As the pH increases, the dye becomes increasingly deprotonated. Furthermore, at lower pH levels, the reduced color removal may indicate the presence of a positive charge forming on the FNAC surface, which hinders the dye removal process. When the pH increases, the oxygen-containing functional groups on the surface of FNAC get deprotonated, leading to a rise in the negative charge on the FNAC surface. Due to the enhanced electrostatic attraction between FBAC and MG, the adsorption of MG got increased[32,34]. Almost similar findings has been reported by Zang et al. for the adsorption of methylene blue on the activated carbon derived by fox nut shell[41].

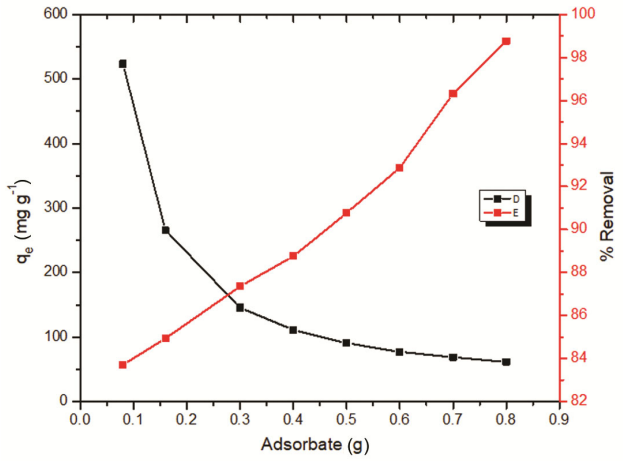

Fig. 4 — Influence of FNAC dose on % removal and adsorption capacity of MG at [MG] = 500 mg/L, pH = 6.5 ± 0.1, Temperature = 298 K, and Contact time = 140 min

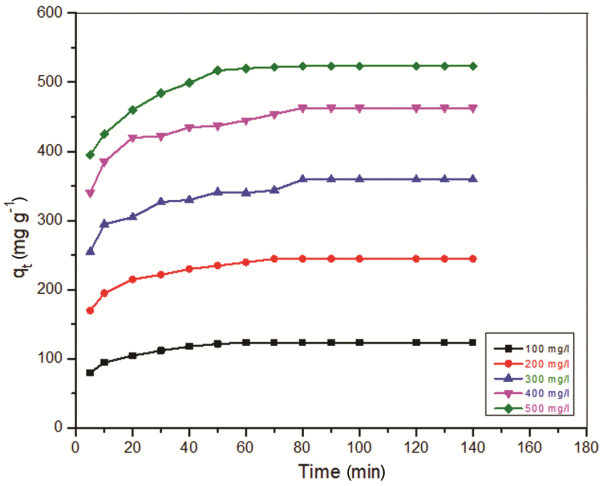

Fig. 5 — Influence of [MG] and contact time on % removal of MG at FNAC dose = 0.08 g/100 ml, pH = 6.5 ± 0.1, Temperature = 298 K, and Contact time = 140 min

Influence of FNAC Dose on MG Removal

The amount of adsorbent utilized is one of the most crucial variables that affects how well the adsorption process goes. Removal effectiveness usually increases with an increase in the adsorbent dosage. The FNAC dose was adjusted between 0.8 and 8.0 g/L in order to discover the optimal adsorbent value for MG removal. Fig. 4 illustrates that the elimination of MG improves from 83.7% to 98.8%, while the adsorption capacity decreases from 523.3 mg/g to 61.7 mg/g as the FNAC dose is raised from 0.8 to 8.0 g/L. With an increase in adsorbent doses, the adsorbent's large surface area and more active adsorbing sites (more availability of functional groups) are responsible for the increase in adsorption effectiveness[43]. Kalita et al. have obtained nearly comparable results regarding the adsorption of basic Fuchsin dye on activated carbon made from Euryale ferox Salisbury seed shell[40].

Influence of Contact Time and Dye Concentration on MG removal

Adsorption, a time-dependent phenomenon, is critical in the design of innovative adsorption systems. The temporal interplay between dyes and adsorbents facilitates the elucidation of the kinetic propensity for binding and sequestration of dyes, alongside the identification of the optimal time range for achieving maximal removal efficiency. The observed trend in the adsorption capacity of MG on FNAC as an indicator of contact time at distinct dye concentrations (100 mg/L to 500 mg/L) is depicted in Fig. 5. It required 70 min for MG with levels ranging from 100 to 200 mg/L to achieve equilibrium. Nevertheless, when dealing with higher concentrations of MG (300–500 mg/L), an extended equilibrium time of 90 min was observed. Initially, it has been observed that the adsorption rate exhibits a rapid increase during the initial time. Subsequently, the rate experiences a gradual increase until reaching 90 min, at which point it stabilizes, indicating the attainment of adsorption equilibrium. The initial swift adsorption can be attributed to the robust affinity between the MG and the FNAC's active sites[33, 34]. As the procedure advanced, the rate of adsorption reduced because the active sites of FNAC were gradually being occupied. The saturation of the FNAC's active sites is what causes the consistency in the adsorption rate.

The starting dye concentration is vital for determining the rate of adsorption to ensure effectiveness. The percentage removal of MG declines from 98.8% to 83.7%, while the adsorption capacity increases from 123.5 mg/g to 523.3 mg/g, as the MG concentration increases from 100 mg/L to 500 mg/L. (Fig. 5). This is because the FNAC dosage was constant, which limited the total number of accessible active sites of FNCA and decreased the percentage of MG removal[32].

Adsorption Isotherms

To explore the adsorption and the mechanisms involved during the process, researchers utilized Freundlich and Langmuir adsorption isotherm models to analyze the MG adsorption evidence on FNCA.

According to the Langmuir isotherm, there is homogeneous adsorption, no adsorbate migration, and monolayer adsorption on a surface with finite adsorption sites. At equilibrium, the Langmuir adsorption equation for a monolayer of adsorbate adsorbed onto the

adsorbent surface with finite active sites can be expressed as[44]:

$$\frac{C_e}{q_e} = \frac{1}{q_{max}K_L} + \frac{C_e}{q_{max}} \quad ...(4)$$

Where,the Langmuir constant is K_L (l/mg), the monolayer adsorbate adsorption performance or capacity is q_{max} (mg/g); The concentration of MG in solution at equilibrium is Ce (mg/l), and q_e (mg/g) denotes the quantity of MG adsorbed on FNAC at equilibrium. Langmuir constant is associated with the free energy of adsorption. Fig. 6 depicts a plot of C_e vs C_e/q_e, exhibiting a linear pattern. The K_L and q_{max}values can be determined by examining the intercept (1/ q_{max} K_L) and slope (1/ q_{max}) of the plot. These values are recorded in Table 1. The linearity observed in the plot depicted in Fig. 6 serves as evidence supporting the validity of the Langmuir model. The experimental findings aligned with the Langmuir model, suggesting the homogeneous nature of the FNAC surface. This observation further demonstrated that a single layer of MG molecule was adsorbed to the external FNAC surface. A similar finding has been documented regarding the MG dye adsorption onto activated carbon produced using various agricultural wastes[27-35]. The outcomes of our investigation's calculation of the monolayer adsorption performance or capacity are superior to those of the previously published work[27-35]. Table 2 provides a comparison of the current work's monolayer adsorption capacity values with those found in the literature.

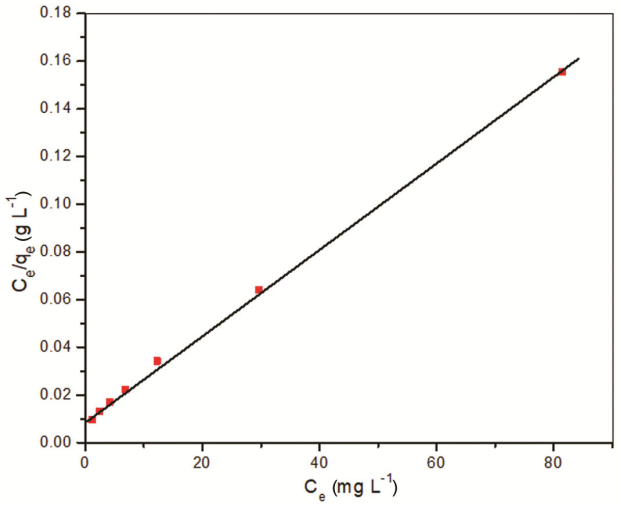

Fig. 6 — Plot of Langmuir isotherm model for the adsorption of MG on FNAC

Table 1 — Langmuir, and Freundlich isotherm constants for the MG adsorption onto FNAC

Isotherm	Constant Values
Langmuir	q_{max}(mg g^{-1}) = 534.7
	R^2 = 0.9984
	R_L= 0.001995
	K_F(mg g^{-1}) = 138.87
Freundlich	1/n = 0.3402
	R^2 = 0.9386

The following equation is used to define a dimensionless equilibrium parameter R_L, which is used to assess the adsorption's favourability:

$$R_L = \frac{1}{1 + K_L C_o} \quad ...(5)$$

Where the initial concentration of MG is C_o (mg/l), and the Langmuir constant is K_L (l/mg). The isotherm type can be classified as irreversible (R_L> 1), unfavourable (R_L = 0), linear (R_L = 1), or favourable (0 < R_L< 1) based on the R_L value[45].

The Freundlich model is suited to highly heterogeneous surfaces and multi-layer adsorption with no plateau. Equation 6 provides the formula for the Freundlich adsorption isotherm[46].

$$log q_e = log K_F + \frac{1}{n} log C_e \quad ...(6)$$

Where Ce (mg/l) is the MG equilibrium concentration, n and KF are Freundlich constants, and qe (mg/g) indicates the quantity of adsorbed MG on FNAC at equilibrium. The linear aspect of the

Table 2 — Comparative studies of the MG adsorption capacities onto various adsorbents

Adsorbent	q_{max} (mg g^{-1})	Reference
Lantana camara L. stem	100.00	27
Nutraceutical industrial fenugreek seed	105.00	28
Okra stalks waste	99.63	29
Stipatenacissima L.) leaf powder	110.98	30
Cocos nucifera shells	32.79	31
Walnut shells	154.56	23
Heveabrasiliensis root	259.49	32
Catha edulis stem	5.62	21
Salaccazalacca	69.44	33
Almond Shell	166.66	34
Jackfruit peel	376.33	35

plot between lnC_e and lnq_e is illustrated in Fig. 7. Table 1 shows the values of n and K_F, which were computed utilizing the intercept (ln K_F) and slope (1/n) of the graph. The value of n indicates the adsorption's favourability. There is a typical Langmuir isotherm if the value of 1/n is smaller than 1[47].

The MG adsorption onto FNAC exhibited excellent conformity to the Langmuir isotherm model, as evidenced by the high R^2 value of 0.9984. This outcome can be attributed to the uniform dispersion of active sites across the FNAC surface. Moreover, the observed R_L values for the Langmuir isotherm fell within the range of 0 to 1, while the Freundlich constant 1/n exhibited a value less than 1, thereby suggesting a process that is thermodynamically favourable[40]. Table 2 displays a comparative examination of MG's adsorption capacity in relation to various activated carbons derived from solid waste materials. The significant adsorption capacity exhibited by this paper elucidates the potential utilization of FNAC as an attractive adsorbent for efficient MG removal. A comparable Langmuir isotherm model has been documented by other scholars concerning the adsorption of cationic dyes onto activated carbon sourced from fox nut shell[40, 41].

Adsorption Kinetics

The kinetic investigation for MG adsorption onto FNAC has been done utilizing Lagergren's first-order model, Ho-McKay's second-order kinetic model, and the intraparticle diffusion model.

Pseudo-first-order model, which is often provided by Eq. 7, is dependent on the solid adsorbent capacity[48].

$$log(q_e - q_t) = logq_e - \frac{k_1}{2.303} t \quad ...(7)$$

Where, q_t (mg/g) and q_e(mg/g)denotes the quantity of MG adsorbed on FNAC at time t and at equilibrium, respectively and the adsorption rate constant is k_1 (min^{-1}). Fig. 8 displays a plot of log ($q_e - q_t$) vs time (t), which has been used to compute the values of the adsorption rate constant (k_1). Table 3 provides a summary of every parameter that was computed with this model. In light of the regression

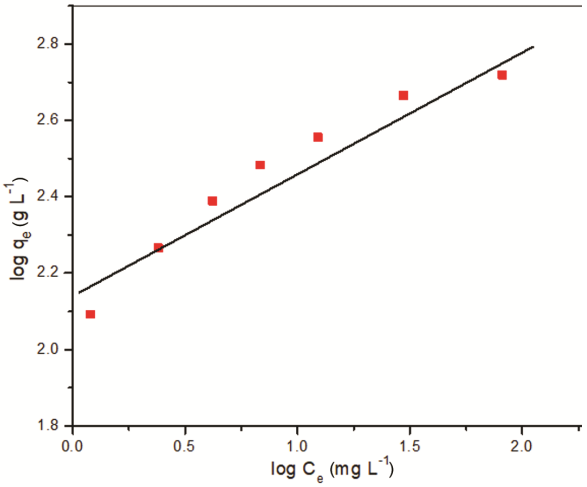

Fig. 7 — Plot of Freundlich isotherm model for the adsorption of MG on FNAC

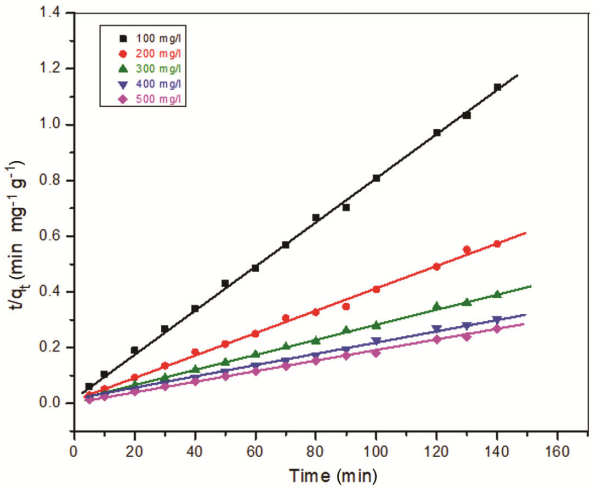

Fig. 8 — Pseudo-first order plot for adsorption of MG on FNAC

Table 3 — Parameters for Pseudo-first order, Pseudo-second order, and Intra-particle diffusion kinetic model

Kinetic Models	Parameters	Initial Dye Concentration (mg/L)				
		100	200	300	400	500
Pseudo-first order kinetic	q_e (mg g^{-1})	67.2	85.5	92.7	115.4	231.3
	k_1 (min^{-1})	0.0687	0.0458	0.0267	0.0333	0.0698
	R^2	0.9565	0.9758	0.9490	0.9446	0.09675
Pseudo-second order kinetic	q_e (mg g^{-1})	127.8	238.1	370.4	454.5	537.6
	k_2 (g^{-1} mg^{-1} min^{-1})	0.00219	0.00142	0.00080	0.00091	0.00064
	R^2	0.0089	0.9967	0.9987	0.9981	0.9983
Intra-particle diffusion model	Intercept	86.38	178.63	261.92	353.92	403.37
	k_p (mg g^{-1} $min^{-0.5}$)	3.822	6.6977	9.5624	10.804	12.233
	R^2	0.7411	0.7940	0.8590	0.8211	0.7856
q_e (mg g^{-1}) [Experimental]		123.5	244.8	359.6	463.0	523.3

coefficient's (R^2) lower values, it appears that this model is not providing the best fit and may not be suitable for the current conditions.

Based on equilibrium adsorption, the pseudo-second-order model has been presented as[49]:

$$\frac{t}{q_t} = \frac{1}{k_2 q_e^2} + \frac{t}{q_e} \quad ...(8)$$

where, k_2 (g/mg min), q_e (mg/g), and q_t (mg/g) are the pseudo-second-order rate constant, amount of MG adsorbed on FNAC at equilibrium and at different times respectively. Fig. 9 illustrates the linear relationship between t/q_t and time t. The values of q_e and k_2 can be found on this graph by using the slope and intercept, respectively. Table 3 has the calculated values listed.

Upon comparing the outcomes of the regression coefficients, it is observed that R^2 exhibited a value of 0.9989 when considering the second-order reaction kinetics. Conversely, when considering the first-order reaction kinetics, R^2 displayed a value of 0.9446. Moreover, the adsorption capacity calculated with the second-order kinetics model (537.6 mg g^{-1}) closely matches the experimental value (523.3 mg g^{-1}) in comparison to the first-order model (231.3 mg g^{-1}). These outcome demonstrate that the adsorption kinetics of MG on FNAC adhere to the principles of second-order kinetics.

The expression for intraparticle diffusion can be represented as[50]:

$$q_t = k_p t^{1/2} + C \quad ...(9)$$

Where Kp represents the intraparticle diffusion rate constant, while C stands for the intercept. The plot of q_t against the $t^{1/2}$ showed a linear relationship (at lower dye concentration) as per the model (Fig. 10). Analysis of the data revealed that the linear lines did not intersect at the origin, suggesting that intraparticle diffusion might not be the primary limiting mechanism for the MG adsorption on the FNAC surface. Table 3 displays the kp, R^2, and C values computed from these plots. R^2 values were lower than the projections generated by the pseudo-second-order model, indicating a lack of agreement with the intraparticle diffusion model. Other studies developed a similar second order kinetic model for the adsorption of cationic dyes on fox nut shell-derived activated carbon[40, 41].

Thermodynamic Studies

The investigation of how temperature affects experimental conditions has also been crucial. The

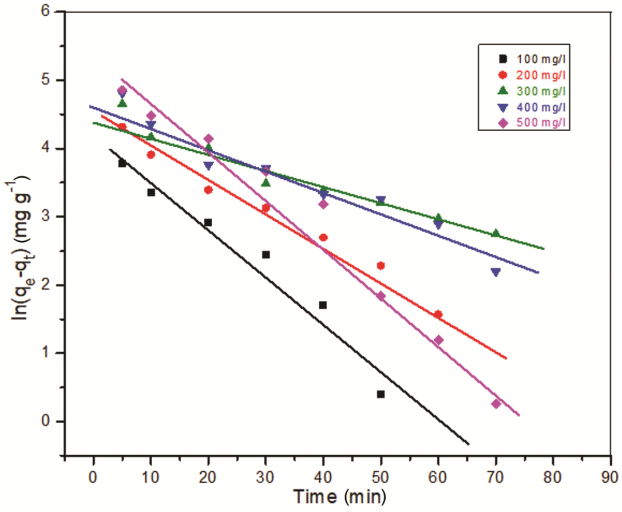

Fig. 9 — Pseudo-second order plot for adsorption of MG on FNAC

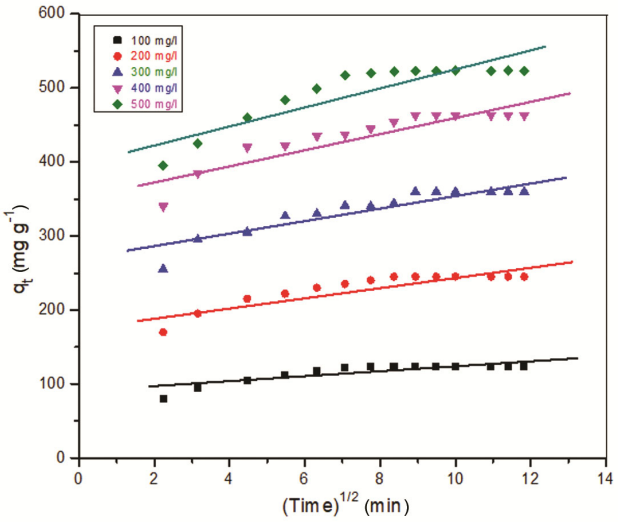

Fig. 10 — Intraparticle diffusion plot for adsorption of MG on FNAC

Table 4 — Thermodynamic parameters for MG adsorption onto FNAC

Temp (K)	$\Delta H^{\#}$ (kJ mol^{-1})	$\Delta S^{\#}$ (J K^{-1} mol^{-1})	$\Delta G^{\#}$ (kJ mol^{-1})
298			- 7.113
303	- 47.263	-134.57	- 6.378
308			- 5.815

temperature effect on the % removal of MG is depicted in Table 4. With the increase in temperature, the % removal and adsorption capacity of MG onto FNAC significantly decreases.

Eq. 10-12 was used to evaluate the thermodynamic activation parameters. Eq. 10 provides the relationship between the equilibrium constant K_D and standard Gibbs free energy ($\Delta G°$) at any temperature T.

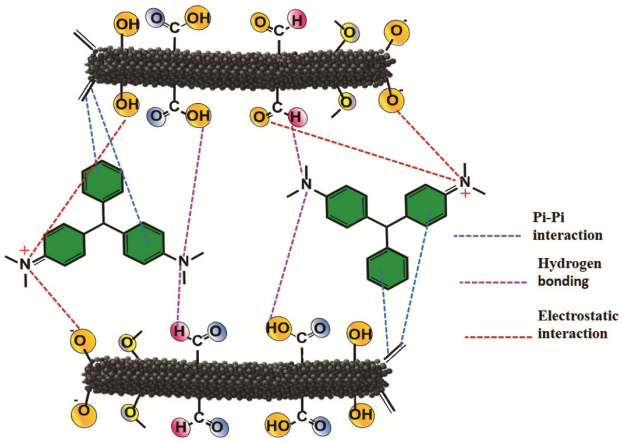

Fig. 11 — Mechanism of adsorption of MG dye on the FNAC surface

$$\Delta G° = -RT \ln K_D \quad ...(10)$$

Eq. 11 provides the relationship between the enthalpy (ΔH°) and entropy (ΔS°) of adsorption with the standard free energy change (ΔG°), while Eq. 12 defines K_D.

$$lnK_D = -(\frac{\Delta G^o}{RT}) = -(\frac{\Delta H^o}{RT}) + \left(\frac{\Delta S^o}{R}\right) \quad ...(11)$$

$$K_D = \frac{C_{Ae}}{C_e} \quad ...(12)$$

Where the equilibrium concentration of MG is C_e, and the quantity of MG adsorbed on FNAC at equilibrium is C_{Ae}. The calculated values of the various parameters have been summarized in Table 4. The adsorption of MG onto FNAC appears to be exothermic, as indicated by the negative value of ΔH°. Furthermore, the negative ΔG° suggests that the adsorption of MG onto FNAC occurs spontaneously. Understanding the exothermic nature of adsorption helps to identify physical adsorption, resulting in a reduction in the adsorption of MG onto FNAC as the temperature rises. Adsorption becomes less favorable at elevated temperatures, as evidenced by the decreasing ΔG° values with a rise in temperature. After the dye has been adsorbed, the solid-solution interface's randomness decreases, as indicated by the negative ΔS° value. For the adsorption of methylene blue on the activated carbon made from fox nut shell, Zang et al. have noted nearly identical results[41].

Mechanism of Adsorption

The elimination of MG dye from the aquatic solution utilizing activated carbon produced from fox nutshell depends extensively on the different functional groups (aromatic, carbonyl, phenol, hydroxyl, etc) present on the surface of FNAC. This was validated by the FTIR spectral analysis shown in Fig. 2. FNAC functional group's surface can be neutral or charged (positive and negative) depending on deprotonation and protonation. Fig. 11 summarizes the potential adsorption pathway of MG dye on the FNAC surface. A variety of interactions, including π–π interactions, hydrogen bonding, and electrostatic attractions among the adsorbate and adsorbent, contribute to the probable adsorption mechanisms between the malachite green dye and FNAC surface functional groups. A similar discovery was made about the MG adsorption on activated carbon developed from Heveabrasiliensis root, rice husk, and Catha edulis stem that had been chemically modified[21, 32, 51].

Conclusion

Current research examines MG adsorption on chemically modified activated carbon derived from fox nutshell (FNAC) in aqueous medium. For optimal adsorption of MG(500 mg/L) onto FNAC (0.8 g/L), a pH value of 6.5 was determined to be the most effective, with an adsorption capacity of 523.3 mg/g at 25°C. The MG adsorption on FNAC occurred rapidly, reaching equilibrium within 90 min. The adsorption proceeds according to pseudo-second-order kinetics, and the Langmuir isotherms provide a good fit for the equilibrium data. Adsorption of MG onto FNAC occurs spontaneously and decreases with temperature, as indicated by negative ΔG° and ΔH°. Possible adsorption mechanisms between FNAC surface functional groups and malachite green dye include π–π interactions, hydrogen bonding, and electrostatic attractions. Overall, the study suggests that the developed adsorbent is suitable for the cost-effective and efficient removal of MG dye from wastewater.

References

1 Prakash S & Verma A K, Arsenic: It's toxicity and impact on human health, *Int J Biol Innov*, 3 (2021) 38.
2 Dahiya V, Heavy metal toxicity of drinking water: A silent killer, *GSC Biol Pharm Sci*, 19 (2022) 20.
3 Sharma R, Agrawal P R, Kumar R & Gupta G, Biosorption for eliminating inorganic contaminants (IOCs) from wastewater, *Biosorp Wastewater Contam*, (2022) 42.
4 Yasasve M, Manjusha M, Manojj D, Hariharan N, Preethi P S, Asaithambi P, Karmegam N, & Saravanan M, Unravelling the emerging carcinogenic contaminants from industrial waste water for prospective remediation by electrocoagulation-A review, *Chemosphere*, 307 (2022) 136017.

5 Ardila-Leal L D, Poutou-Piñales R A, Pedroza-Rodríguez A M & Quevedo-Hidalgo B E, A brief history of colour the environmental impact of synthetic dyes and removal by using laccases, *Molecules*, 26 (2021) 3813.

6 Dassanayake R S, Acharya S & Abidi N, Recent advances in biopolymer-based dye removal technologies, *Molecules*, 26 (2021) 4697.

7 Elgarahy A, Elwakeel K, Mohammad S & Elshoubaky G, A critical review of biosorption of dyes heavy metals and metalloids from wastewater as an efficient and green process, *Chem Eng Technol*, 4 (2021)100209.

8 Selvaraj V, Karthika T S, Mansiya C & Alagar M, An over review on recently developed techniques mechanisms and intermediate involved in the advanced azo dye degradation for industrial applications, *J Mol Struct*, 1224 (2021) 129195.

9 Ikram M, Zahoor M & Batiha G E S, Biodegradation and decolorization of textile dyes by bacterial strains: A biological approach for wastewater treatment, *Z fur Phys Chem*, 235 (2021) 1381.

10 Hamzezadeh A, RashtbariY, Afshin S, Morovati M & Vosoughi M, Application of low-cost material for adsorption of dye from aqueous solution, *J Environ Anal Chem*, 102 (2022) 254.

11 Rathi B S, Kumar P S & Vo D V N, Critical review on hazardous pollutants in water environment: Occurrence monitoring fate removal technologies and risk assessment, *Sci Total Environ*, 797 (2021) 149134.

12 Kutluay S, Excellent adsorptive performance of novel magnetic nano-adsorbent functionalized with 8-hydroxyquinoline-5-sulfonic acid for the removal of volatile organic compounds (BTX) vapors, *Fuel*, 287 (2021) 119691.

13 Goswami M K, Srivastava A, Dohare R K, Tiwari A K & Srivastava A, Recent advances on conducting polymer based magnetic nanosorbents for dyes and heavy metal removal: Fabrication applications and perspective, *Environ Sci Pollut Res*, 30 (2023) 3031.

14 Sudha M, Saranya A & Selvakumar G, Microbial degradation of azo dyes: A review, *Int J Curr Microbiol App Sci*, 3 (2014) 670.

15 Baban A, Yediler A & Lienert D, Ozonation of high strength segregated effluents from a woollen textile dyeing and finishing plant, *Dyes Pigm*, 58 (2023) 93.

16 Hassani A, Çelikdağ G, Eghbali P, Sevim M, Karaca S & Metin Ö, Heterogeneous sono-Fenton-like process using magnetic cobalt ferrite-reduced graphene oxide ($CoFe_2O_4$-rGO) nanocomposite for the removal of organic dyes from aqueous solution, *Ultrason Sonochem*, 40 (2018) 841.

17 Oladoye P O, Ajiboye T O, Wanyonyi W C, Omotola E O & Oladipo M E, Insights into remediation and decontamination technology of malachite green wastewater, *Water Sci Eng*, 16 (2023) 261.

18 Mosebolatan J, Ayorinde M & Adelaja Y, Results in engineering valorization of microwave-assisted H_3PO_4-activated plantain (Musa paradisiacal L) leaf biochar for malachite green sequestration: Models and mechanism of adsorption, *Results Eng*, 18 (2023) 101129.

19 Bhat S S, Narayana B & Bhat J I, Adsorption of malachite green dye using low-cost adsorbent derived from java apple leaves (Syzyiumsamarangense), *Sādhanā*, 48 (2023) 0123456789.

20 Lemos E S, Fiorentini E F, Bonilla-petriciolet A & Escudero L B, Malachite green removal by grape stalks biosorption from natural waters and effluents, *Adsorp Sci Technol*, (2023) 6695937.

21 Abate G Y, Alene A N, Habte A T & Getahun D M, Adsorptive removal of malachite green dye from aqueous solution onto activated carbon of Catha edulis stem as a low cost bio-adsorbent, *Environ Syst Res*, 9 (2020) 29.

22 He J, Mo P, Luo Y & Yang P, Strategies for solving the issue of malachite green residues in aquatic products: A review, *Aquacult Res*, (2023) 8578570.

23 Merrad S, Abbas M & Trari M, Adsorption of malachite green onto walnut shells: Kinetics, thermodynamic, and regeneration of the adsorbent by chemical process, *Fibers Polym*, 24 (2023) 1067.

24 Muttil N, Jagadeesan S, Chanda A, Duke M & Singh S K, Production, types, and applications of activated carbon derived from waste tyres: An overview, *Appl Sci,* 13 (2023) 257.

25 Wang B, Lan J, Bo C, Gong B & Ou J, Adsorption of heavy metal onto biomass-derived activated carbon: A review, *RSC Adv*, 13 (2023) 4275.

26 Ani J U, Akpomie K G & Okoro U C, Potentials of activated carbon produced from biomass materials for sequestration of dyes, heavy metals, and crude oil components from aqueous environment, *Appl Water Sci*, 10 (2020) 69.

27 Samimi M, Shahriari-Moghadam M & Te-Lantana C L, Stem biomass as an inexpensive and efficient biosorbent for the adsorptive removal of malachite green from aquatic environments: Kinetics, equilibrium and thermodynamic studies, *Int J Phytoremediat*, 25 (2023) 1328.

28 Taqui S N, Mohan C S & Khatoon B A, Sustainable adsorption method for the remediation of malachite green dye using nutraceutical industrial fenugreek seed spent, *Biomass Convers Biorefin*, 13 (2023) 9119.

29 Yildiz H, Gülşen H, Şahin Ö, Baytar O & Kutluay S, Novel adsorbent for malachite green from okra stalks waste: Synthesis, kinetics and equilibrium studies, *Int J Phytoremediat*, 10 (2023) 1.

30 Violet C, Stipa A & Alghyamah A, Biosorption of triphenyl methane dyes (malachite green and crystal violet) from aqueous media by Alfa (Stipatenacissima L.) leaf powder, *Molecules*, 28 (2023) 3313.

31 Priaya R S, Jayabalakrishnan R M, Maheswari M, Boomiraj K & Oumabady S, Comparative adsorption study of malachite green dye on acid-activated carbon, *Int J Environ Anal Chem*, 103 (2023) 16.

32 Ahmad A A, Ahmad M A, Yahaya N K E M & Karim J, Adsorption of malachite green by activated carbon derived from gasified *Hevea brasiliensis* root, *Arabian J Chem*, 14 (2021) 103104.

33 Hasanah M, Wijaya A, Arsyad F S, Mohadi R & Lesbani A, Preparation of C-based magnetic materials from fruit peel and hydrochar using snake fruit (Salaccazalacca) peel as adsorbents for the removal of malachite green dye, *Environ Nat Resour*, 21 (2023) 67.

34 Chouli F, Ezzat A O, Sabantina L, Benyoucef A & Zehhaf A, Optimization conditions of malachite green adsorption onto almond shell carbon waste using process design, *Molecules*, 29 (2023) 54.

35 Yusop M F M, Abdullah A Z & Ahmad M A, Malachite green dye adsorption by jackfruit based activated carbon: Optimization, mass transfer simulation and surface area prediction, *Diam Relat Mater*, 136 (2023) 109991.
36 Abewaa M, Mengistu A, Takele T, Fito J & Nkambule T, Adsorptive removal of malachite green dye from aqueous solution using Rumexabyssinicus derived activated carbon, *Sci Rep*, 13 (2023) 14701.
37 Das S, Raychaudhuri U & Maulik N, The effect of Euryale ferox (Makhana), an herb of aquatic origin, on myocardial ischemic reperfusion injury, *Mol Cell Biochem*, 289 (2006) 55.
38 Kumar A & Jena H M, High surface area microporous activated carbons prepared from fox nut (Euryale ferox) shell by zinc chloride activation, *Appl Surf Sci*, 356 (2015) 753.
39 Kumar A & Jena H M, Preparation and characterization of high surface area activated carbon from fox nut (Euryale ferox) shell by chemical activation with H_3PO_4, *Results Phys*, 6 (2016) 651.
40 Kalita S, Pathak M & Devi G, Utilization of Euryale feroxsalisbury seed shell for removal of basic fuchsin dye from water: Equilibrium and kinetics investigation, *RSC Adv*, 44 (2017) 27248.
41 Zhang H, Liu Y, Wu X, Jin X, Zhang Z, Zhao H, Liu J, Huang Z, Fang M & Min X, Kinetics and equilibrium studies of the adsorption of methylene blue on Euryale ferox shell-based activated carbon, *Micro Nano Lett, 13 (2018)* 552.
42 Ryu Z, Zheng J, Wang M & Zhang B, Characterization of pore size distributions on carbonaceous adsorbents by DFT, *Carbon*, 37 (1999) 1257.
43 Tee G T, Gok X Y & Yong W F, Adsorption of pollutants in wastewater via biosorbents, nanoparticles and magnetic biosorbents: A review, *Environ Res*, 212 (2022) 113248.
44 Langmuir I, The adsorption of gases on plane surfaces of glass, mica and platinum, *J Am Chem Soc*, 40 (1918) 1361.
45 Weber T W & Chakkravorti R K, Pore and solid diffusion models for fixed bed adsorbers, *Am Inst Chem Eng J*, 20 (1974) 228.
46 Freundlich H, Adsorption in solution, *Phys Chem Soc*, 40 (1906) 1361.
47 Temkin M I & Pyzhev V, Kinetic of ammonia synthesis on promoted iron catalysts, *Acta Physiochim URSS*, 12 (1940) 327.
48 Kalavathy M H, Karthikeyan T & Rajgopal S, Kinetic and isotherm studies of Cu(II) adsorption onto H_3PO_4-activated rubber wood sawdust, *J Colloid Interf Sci*, 292 (2005) 354.
49 Li Y H, Di Z C, Ding J, Wu D H, Luan Z K & Zhu Y Q, Adsorption thermodynamic, kinetic and desorption studies of Pb_2+ on carbon nanotubes, *Water Res*, 39 (2005) 605.
50 Weber W J & Morris J C, Kinetics of adsorption on carbon from solution, *J Sanit Eng Div,* 89 (1963) 31.
51 Chowdhury S, Mishra R, Saha P & Kushwaha P, Adsorption thermodynamics, kinetics and isosteric heat of adsorption of malachite green onto chemically modified rice husk, *Desalination*, 265 (2011) 159.